IOP Publishing Physica Scripta
Phys. Scr. **81** (2010) 045007 (13pp) doi:10.1088/0031-8949/81/04/045007

Spatiotemporal chaos in coupled logistic maps

Andre Varella Guedes and Marcelo Amorim Savi

Universidade Federal do Rio de Janeiro, COPPE - Department of Mechanical Engineering, PO Box 68.503, 21.941.972, Rio de Janeiro, RJ, Brazil

E-mail: savi@mecanica.ufrj.br

Received 9 September 2009
Accepted for publication 18 February 2010
Published 19 March 2010
Online at stacks.iop.org/PhysScr/81/045007

Abstract
The objective of this work is to investigate the spatiotemporal dynamics of coupled logistic maps. These maps are prototypes of high-dimensional dynamical systems and have been used to describe the evolution and pattern formation in different systems. Here, the logistic map lattice is coupled by a power law and, therefore, each map is influenced by other maps in its neighborhood. The Kolmogorov–Sinai entropy density is employed to quantify the complexity of system behavior, permitting a general qualitative understanding of different aspects of system dynamics. Three kinds of boundary conditions are treated and the influence of initial conditions is also of concern. Non-homogeneous maps are investigated, showing interesting aspects of spatiotemporal dynamics. The idea is to analyze the spatial interaction between two qualitative different types of behavior from a grid that is split into two parts. Numerical simulations show what types of conditions present a greater tendency to develop chaotic, periodic and synchronized responses. It should be highlighted that non-homogeneous grids have situations where a chaotic pattern can emerge from two periodic responses and also situations where a periodic pattern can emerge from chaos.

PACS numbers: 05.45.-a, 05.45.Jn

(Some figures in this article are in colour only in the electronic version.)

1. Introduction

Natural systems have nonlinear characteristics that are responsible for a great variety of possibilities. Chaos is one of these possibilities, and natural systems can adopt chaotic regimes as desirable behavior due to the intrinsic richness related to the existence of an infinite number of unstable periodic orbits. In the past, most research was dedicated to investigating the temporal evolution of low-dimensional systems. Recently, the spatiotemporal evolution of dynamical systems has increasing importance (Savi 2007, Viana *et al* 2005, Vasconcelos *et al* 2004, Lai and Grebogi 1999, Shibata 1998a, 1998b, Awrejcewicz 1991, Umberger *et al* 1989). The spatiotemporal characteristics of a dynamical system are important in the analysis of complex behavior.

This paper presents an investigation of the spatiotemporal dynamics of coupled maps. The system is composed of a logistic map lattice connected by a communication protocol. This coupling is described by a power law that can represent either local- or global-type couplings. Therefore, each map is influenced by other maps in its neighborhood, and boundary conditions are important in defining the coupling characteristics. This map lattice represents a mathematical idealization of physical systems that are discrete in time and space. It is used to describe the evolution and pattern formation in chemical reactions, turbulence, neural networks and population dynamics. Because of that, the investigation of this system became important in nonlinear dynamics analysis (Wysham and Hastings 2008, Lloyd 1995, Holden and Zhang 1992).

The literature presents numerous investigations concerning coupled logistic maps. Willeboordse (2003) argued that the key motivation is the search for universal properties and behavior that apply to all dynamical systems. Therefore, coupled maps can be understood as prototypes of high-dimensional dynamical systems. Shen *et al* (2008) studied the synchronization and pattern dynamics of coupled logistic maps on a type of complex network,

constructed by randomly adding shortcuts to a regular ring. Li (2008) considered the synchronization of globally coupled maps subjected to a constant force. Kozma (1998) stated that the results obtained for coupled logistic maps with intermediate-range coupling are directly related to the emergence of intelligent behavior in neural networks. Giordani *et al* (2005) investigated the synchronization of metapopulations by means of observing the chaotic behavior of coupled logistic maps.

In general, the synchronization of spatiotemporal dynamics has been intensively studied, but there is a dearth of studies on the systematic investigation of other aspects of system dynamics (Chazottes and Fernandes 2005). In this regard, this contribution investigates the different aspects of system dynamics treating the influence of boundary and initial conditions and also the influence of non-homogeneous effects on system dynamics. The main goal is to present some interesting patterns related to spatiotemporal dynamics. The Kolmogorov–Sinai entropy density is used to quantify the complexity of system behavior permitting a general qualitative comprehension of system dynamics. Entropy surfaces are used to identify different qualitative dynamics that are explored in numerical simulations. Three kinds of boundary conditions are considered: periodic, where the values of the maps are repeated for every N maps; infinite space, where the neighborhoods of the first and last maps have homogeneous values; and finite space, where no other map is considered beyond the N observed. Besides boundary conditions, the influence of initial conditions and non-homogeneous effects is also of concern. The idea of non-homogeneous analysis is to investigate the spatial interaction between two qualitatively different types of behavior from a grid that is split into two parts. Numerical simulations show the types of conditions that present a greater tendency to develop chaotic, periodic and synchronized responses. It should be highlighted that the non-homogeneous grids have situations where chaos can emerge from the interaction of periodic behavior and vice versa.

2. Coupled maps

The logistic map was originally proposed by May (1976) to describe biological problems. Today, this map is employed to describe different problems related to economic and social areas. The logistic map is a first-order difference equation represented by $x_{n+1} = f(\mathrm{x}_n;\beta) = \beta x_n(1-x_n)$. Recently, coupled logistic maps have been used in order to model the evolution and pattern formation in systems associated with chemical reactions, turbulence, neural networks and population dynamics (Holden and Zhang 1992).

The map lattice considers a grid of N logistic maps coupled by a power law as follows (Viana *et al* 2005):

$$x_{n+1}^{(i)} = (1-\varepsilon)\, f\left(x_n^{(i)}\right) + \frac{\varepsilon}{\eta(\alpha)} \sum_{j=1}^{N'} \frac{1}{j^{\alpha}} \left[f\left(x_n^{(i+j)}\right) + f\left(x_n^{(i-j)}\right) \right], \tag{1}$$

where $N' = (N-1)/2$ and $f(x) = \beta x(1-x)$; ε is the coupling parameter ($0 \leqslant \varepsilon \leqslant 1$), α is the coupling intensity ($\alpha \geqslant 0$) and η is given by

$$\eta(\alpha) = 2\sum_{j=1}^{N'} j^{-\alpha}. \tag{2}$$

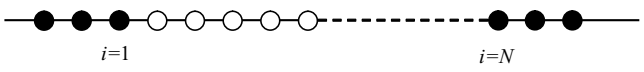

Figure 1. Coupled map grid.

This coupling represents different aspects of the communication protocol and allows a continuous pass from local Laplacian-type coupling ($\alpha \to \infty$) to global mean-field coupling ($\alpha \to 0$) (Viana *et al* 2005).

Each map i depends on its neighbors and the boundary conditions define the maps when $i > N$ and $i < 1$. Figure 1 represents the coupled maps grid, illustrating the boundaries.

Numerous boundary conditions can be established in order to represent distinct physical situations. Here, three different boundaries are of concern. The *periodic* condition is the most usual one observed in the literature, being related to an infinite space where the map values repeat for each N map. Mathematically, this condition is represented by

$$x_n^{(i)} = x_n^{(i\pm N)}. \tag{3}$$

Infinite space is a free boundary condition where the N-lattice behavior is repeated for outside cells. Under this assumption, the map response in $i = N$ repeats its value to the right side of the grid while the values to the left assume the value of the map $i = 1$ (figure 1). The mathematical representation of this condition for the boundary and outer cells is

$$\begin{aligned} x_n^{(N)} &= x_n^{(N+1)} = x_n^{(N+2)} = \cdots = x_n^{(\infty)}, \\ x_n^{(1)} &= x_n^{(0)} = x_n^{(-1)} = \cdots = x_n^{(-\infty)}. \end{aligned} \tag{4}$$

The *finite space* condition represents a situation where the boundary is fixed, vanishing cell responses of maps out of the lattice as follows:

$$\begin{aligned} x_n^{(N)} &= x_n^{(N+1)} = x_n^{(N+2)} = \cdots = x_n^{(\infty)} = 0, \\ x_n^{(1)} &= x_n^{(0)} = x_n^{(-1)} = \cdots = x_n^{(-\infty)} = 0. \end{aligned} \tag{5}$$

3. Lyapunov exponents and Kolmogorov–Sinai entropy density

A Lyapunov spectrum represents one of the most important geometrical invariants of a dynamical system. Lyapunov exponents evaluate the divergence of nearby orbits and their signs provide a qualitative picture of the system's dynamics. Any system containing at least one positive exponent presents chaotic behavior. The analysis of coupled maps can use the same methodology employed for a single map. Hence, let us assume coupled maps expressed by

$$x_{n+1}^{(i)} = f\left(x_n^{(i)}\right) = f\left(x_n^{(1)}, \ldots, x_n^{(N)}\right). \tag{6}$$

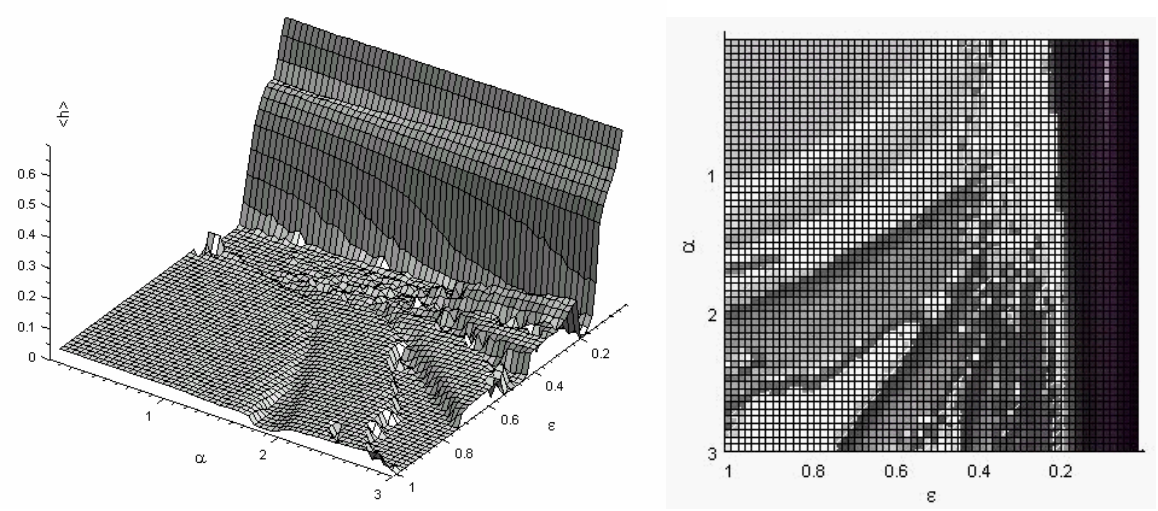

Figure 2. Kolmogorov–Sinai entropy density for periodic boundary conditions and different coupling parameters.

The determination of Lyapunov exponents needs to consider the variation of each cell under some perturbation in initial conditions, $x_0^{(i)}$. The Jacobian matrix is calculated in each iteration as follows (Shibata 2001):

$$J_n = \begin{pmatrix} \frac{\partial x_{n+1}^{(1)}}{\partial x_n^{(1)}} & \frac{\partial x_{n+1}^{(1)}}{\partial x_n^{(2)}} & \cdots & \frac{\partial x_{n+1}^{(1)}}{\partial x_n^{(N)}} \\ \frac{\partial x_{n+1}^{(2)}}{\partial x_n^{(1)}} & \frac{\partial x_{n+1}^{(2)}}{\partial x_n^{(2)}} & \cdots & \frac{\partial x_{n+1}^{(2)}}{\partial x_n^{(N)}} \\ \vdots & \vdots & \ddots & \vdots \\ \frac{\partial x_{n+1}^{(N)}}{\partial x_n^{(1)}} & \frac{\partial x_{n+1}^{(N)}}{\partial x_n^{(2)}} & \cdots & \frac{\partial x_{n+1}^{(N)}}{\partial x_n^{(N)}} \end{pmatrix}. \tag{7}$$

Then,

$$R_n = \prod_{k=1}^{n} J_k \tag{8}$$

is defined.

Lyapunov exponents, $\lambda^{(i)}$, are evaluated from the eigenvalue $\sigma^{(i)}$ of R_n as follows (Holden and Zhang 1992):

$$\lambda^{(i)} = \lim_{n\to\infty} \frac{1}{n} \ln \left|\sigma^{(i)}\right|. \tag{9}$$

By considering the coupled logistic maps lattice where the coupling is defined by a power law as presented in equation (1), the Jacobian matrix is written as

$$[J_n]_{ij} = A_{ij} f'\left(x_n^{(j)}\right), \tag{10}$$

where A_{ij} is a coupling dependent matrix given by (Batista and Viana, 2001)

$$A_{ij}(\varepsilon,\alpha) = \begin{cases} 1-\varepsilon, & \text{if } i = j, \\ \varepsilon |i-j|^{-\alpha}/\eta(\alpha), & \text{if } |i-j| \leqslant N', \\ \varepsilon (N' - |i-j|)^{-\alpha}/\eta(\alpha), & \text{if } |i-j| > N'. \end{cases} \tag{11}$$

The use of the classical algorithm due to Wolf *et al* (1985) allows the evaluation of the principal directions of the ellipsoid centered at a fiducial trajectory (Lu *et al* 2005). The norms of the orthonormalized vectors $N_k^{(i)}$ are used to calculate the Lyapunov exponents and, after n iterations, we have

$$\lambda_n^{(i)} = \frac{1}{n} \sum_{k=1}^{n} \ln N_k^{(i)}. \tag{12}$$

The knowledge of this spectrum allows one to evaluate other invariants such as the Kolmogorov–Sinai entropy density, which is an index calculated from the positive Lyapunov exponents as follows:

$$h = \frac{1}{N} \sum_{i=1}^{N,\lambda>0} \lambda_i. \tag{13}$$

Hence, when the entropy density vanishes there is no positive Lyapunov exponent and, therefore, there is regular behavior. On the other hand, positive values of the entropy are related to chaos.

4. Homogeneous maps

We now focus on homogeneous coupled lattice maps by assuming a grid with $N = 21$ and $\beta = 4$, which is associated with chaotic behavior of the isolated map. All simulations were conducted assuming that parameter ε is between 0 and 1, and parameter α is between 0 and 3. These choices represent different kinds of couplings, changing from local to global characteristics. The Kolmogorov–Sinai entropy was calculated from converged Lyapunov exponents. Random initial conditions are assumed and three different boundary conditions are of concern: periodic, infinite space and finite space. The idea is to investigate how the coupling characteristics influence the global dynamics.

4.1. Periodic boundary conditions

Initially, let us consider periodic boundary conditions. The analysis of Kolmogorov–Sinai entropy density for different coupling parameter values allows us to identify distinct behavior, as shown in figure 2. This entropy surface characterizes general system dynamics, giving us an idea of coupling effects. Flat regions, related to α values less than

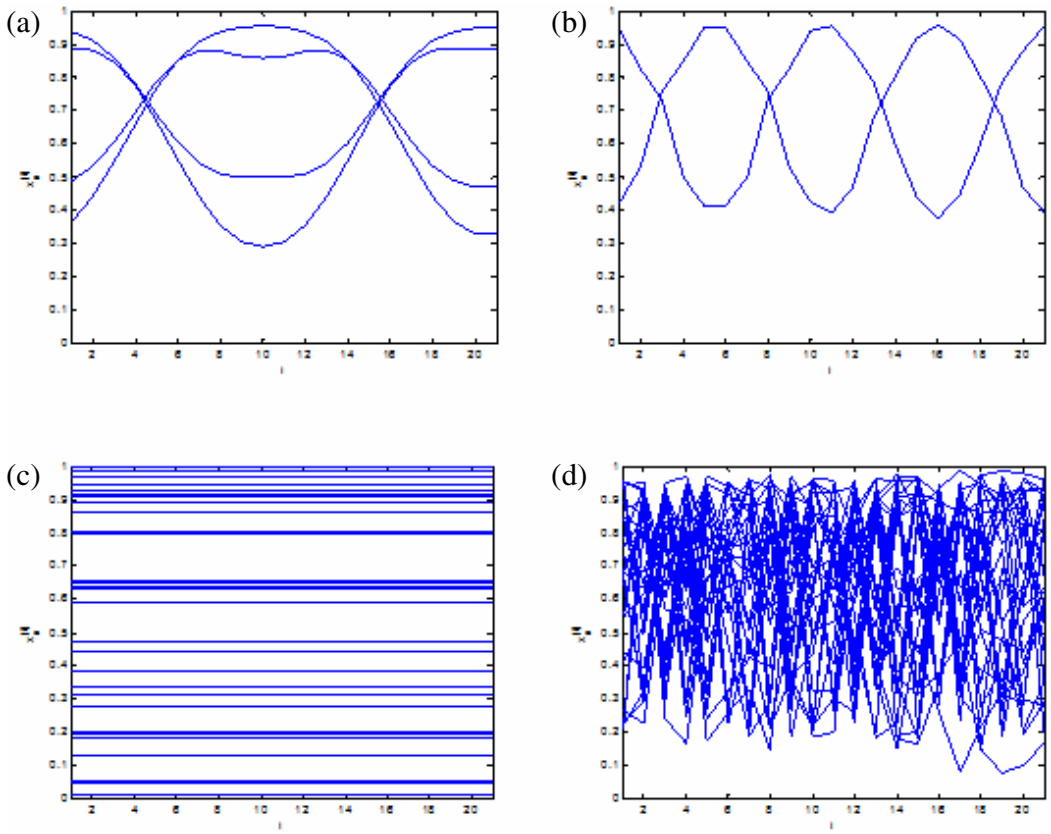

Figure 3. Overlap of the last 30 iterations after 10 000 iterations for periodic boundary response with (a) $\alpha = 1.9$ and $\varepsilon = 1$; (b) $\alpha = 3$ and $\varepsilon = 1$; (c) $\alpha = 1$ and $\varepsilon = 1$; (d) $\alpha = 2$ and $\varepsilon = 0.11$.

1.5 and ε values greater than 0.6, are associated with maps synchronization presenting homogeneous dynamics. This homogeneity, however, is not related to regular dynamics and can be associated with chaos when related to positive entropy values. As expected, the decrease of coupling parameters makes the system response similar to the uncoupled behavior of isolated maps.

For situations when ε is less than 0.2, for all values of α, the system presents chaotic behavior due to the weak coupling and, therefore, the isolated behavior of each map tends to be dominant. Note that the entropy density tends to $h = 0.69$, a value that corresponds to the isolated map. It should also be pointed out that the existence of valleys, where entropy density vanishes, characterizes regular response. For instance, when $\alpha = 1.9$ and $\varepsilon = 1$, the system presents a period-4 response that could be observed from the pattern presented in figure 3(a), which shows the spatiotemporal evolution represented by an overlap of 30 iterations. In the same way, when $\alpha = 3$ and $\varepsilon = 1$, there is a period-2 pattern (figure 3(b)). When $\alpha = 1$ and $\varepsilon = 1$, the system presents a synchronized chaotic response characterized by a consensus response of the whole grid (figure 3(c)). A chaotic pattern is reached when $\alpha = 2$ and $\varepsilon = 0.11$ (figure 3(d)). These results show distinct patterns that emerge from the coupled logistic map.

4.2. Infinite space boundary conditions

A system with infinite space boundary conditions is now considered, meaning that the boundary is free to follow the behavior of the boundary cell. The analysis of Kolmogorov–Sinai entropy density for different coupling parameter values is presented in figure 4. Once again, there is a flat region ($h \approx 0.033$) limited by a valley defined by the pairs $\alpha = 1.7$, $\varepsilon = 1$ and $\alpha = 0.5$, $\varepsilon = 0.4$, but now it is not related to synchronized response. Afterwards, there is another flat region. It is also possible to see some valleys close to $\alpha = 3$ with zero entropy. As expected, when coupled parameters tend to vanish, the response tends to uncoupled

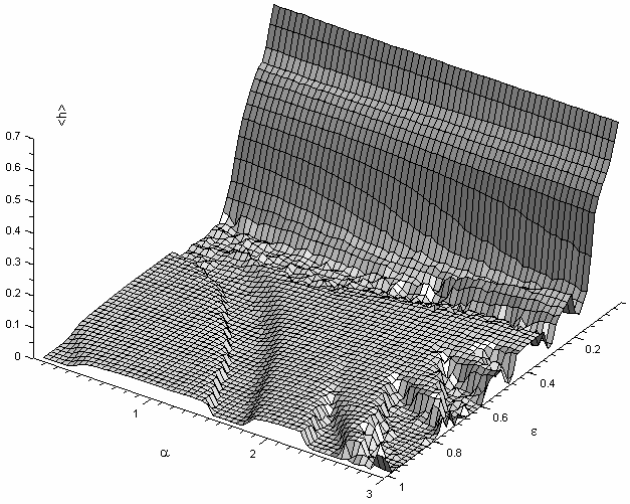

Figure 4. Kolmogorov–Sinai entropy density for infinite space boundary conditions and different coupling parameters.

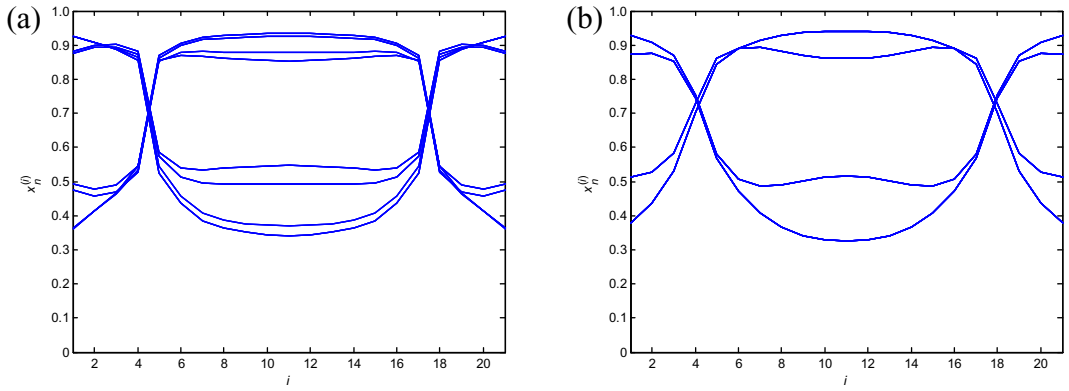

Figure 5. Overlap of the last 30 iterations after 10 000 iterations for infinite boundary response: (a) $\alpha = 0.5$ and $\varepsilon = 0.4$; (b) $\alpha = 1.7$ and $\varepsilon = 1$.

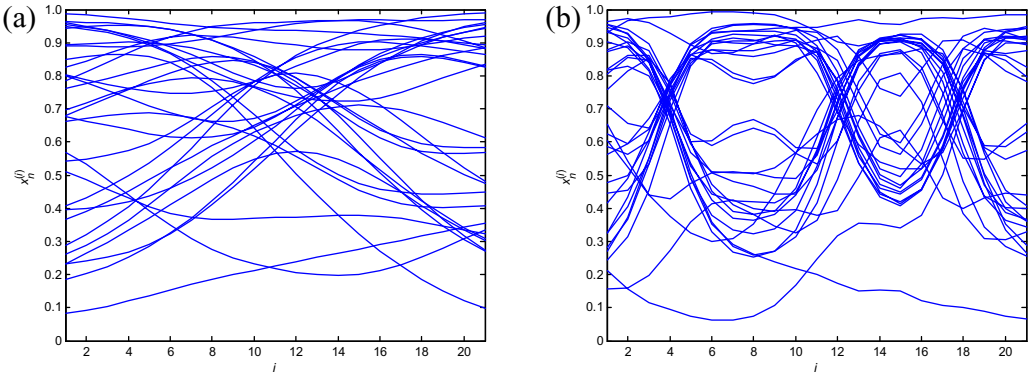

Figure 6. Overlap of the last 30 iterations after 10 000 iterations for infinite space boundary conditions: (a) $\alpha = 0.6$ and $\varepsilon = 0.75$; (b) $\alpha = 1.75$ and $\varepsilon = 0.6$.

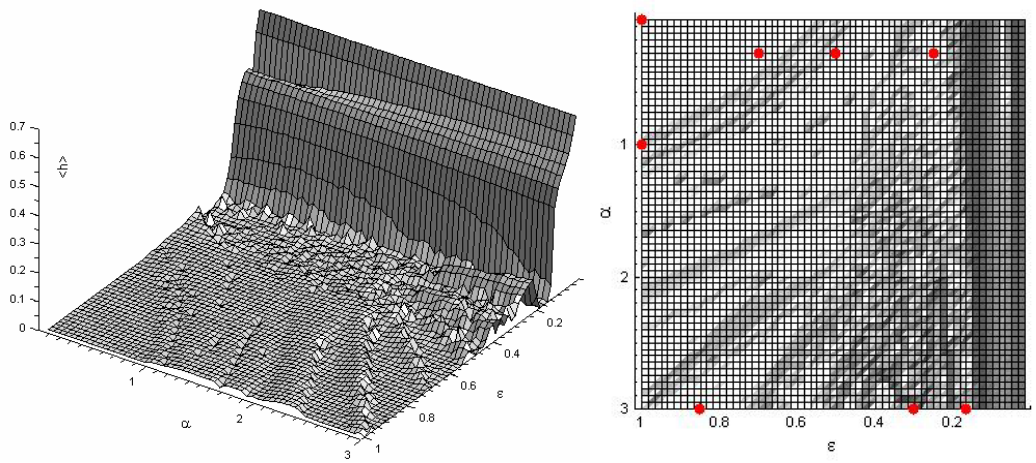

Figure 7. Kolmogorov–Sinai entropy density for finite space boundary conditions and different coupling parameters.

behavior. In general, it should be concluded that boundary conditions have a great influence on the results, and infinite space boundary condition responses have a greater tendency to chaos without synchronization when compared to those obtained with a periodic boundary.

System behavior at the first valley can be visualized by considering two different situations: $\alpha = 0.5$ and $\varepsilon = 0.4$; $\alpha = 1.7$ and $\varepsilon = 1$. Figure 5 presents these results, showing different even periodic response patterns. Regions close to the valleys show a weakly chaotic response, characterized by intermittency. Figure 6 presents the results for $\alpha = 0.5$, $\varepsilon = 0.4$ and $\alpha = 1.7$, $\varepsilon = 1$.

4.3. Finite space boundary conditions

Let us now consider the system with finite boundary conditions by assuming the existence of just 21 maps within the grid, meaning that the outside lattice behavior vanishes. The analysis of the entropy density surface at the coupling parameters space is presented in figure 7. It should be noted

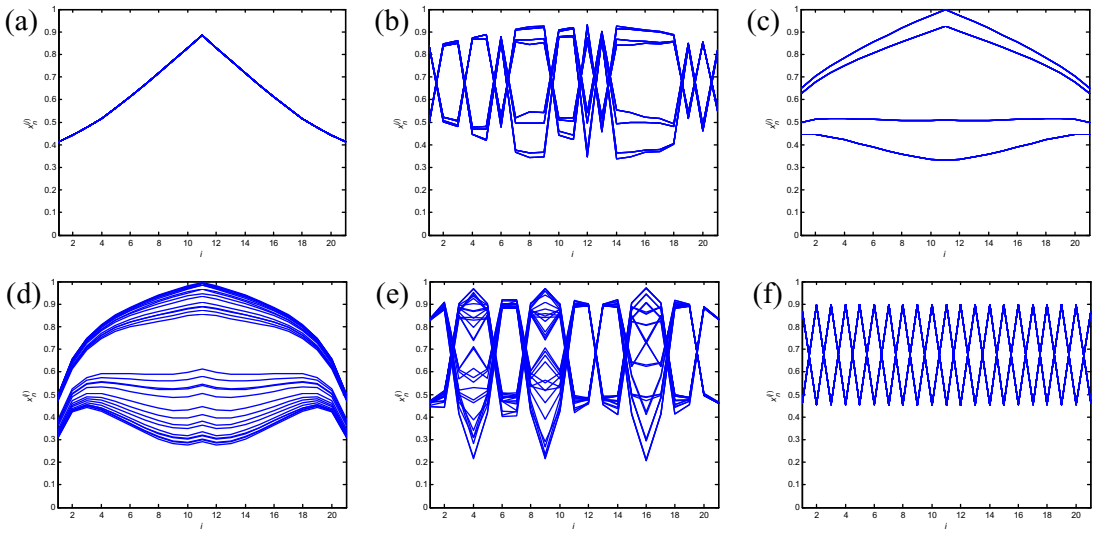

Figure 8. Overlap of the last 30 iterations after 10 000 iterations for finite boundary conditions with different coupling parameters: (a) $\alpha = 0$ and $\varepsilon = 1$; (b) $\alpha = 0.3$ and $\varepsilon = 0.25$; (c) $\alpha = 0.3$ and $\varepsilon = 0.7$; (d) $\alpha = 1$ and $\varepsilon = 1$; (e) $\alpha = 3$ and $\varepsilon = 0.3$; (f) $\alpha = 3$ and $\varepsilon = 0.166$.

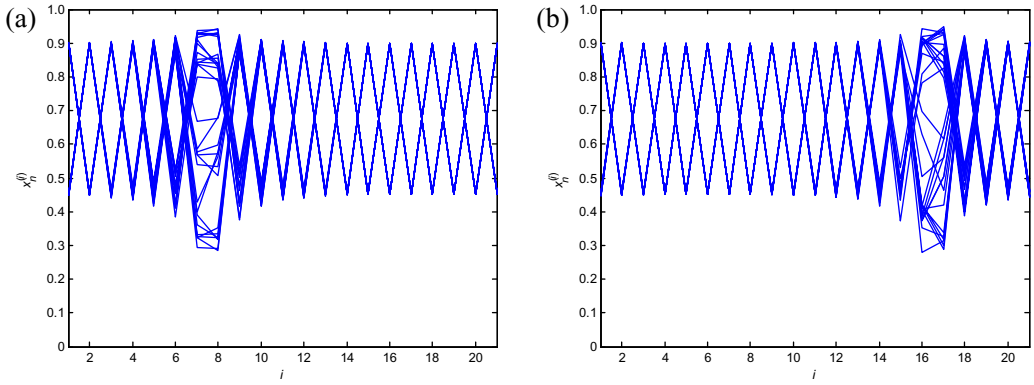

Figure 9. Overlap of the last 30 iterations after 10 000 iterations for periodic boundary response with $\alpha = 3$ and $\varepsilon = 0.165$.

that this system tends to present a great region related to very low values, or a zero value, of entropy and strong chaos is restricted to low values of parameter ε. Figure 8 presents the spatiotemporal evolution for different kinds of responses related to distinct coupling parameters (identified in figure 7), varying from regular to chaotic responses.

4.4. Influence of initial conditions

The influence of initial conditions in system response is now of concern. In order to deal with the spatiotemporal characteristics, let us consider a system with periodic boundary conditions with $\alpha = 3$ and $\varepsilon = 0.165$, presented in figure 9 as an overlap of the last 30 iterations after 10 000 iterations. Two different initial conditions are considered: figure 9(a) is related to homogeneous initial conditions $x_0^{(i)} = 0$, except for $x_0^{(1)} = 0.1$, while figure 9(b) considers $x_0^{(10)} = 0.1$, vanishing all others. Both situations can be understood as a chaotic wave traveling through a period-2 response. The spatiotemporal aspects, however, are altered by the initial conditions.

The analysis of different time instants is useful for the correct comprehension of spatiotemporal dynamics. Figure 10 presents a map showing how the chaotic wave moves itself within the period-2 response. This figure also shows the system spatiotemporal evolution, presenting detailed windows obtained from the overlap of 30 iterations where it is possible to verify the position of the chaotic region.

The infinite space boundary condition is now considered by assuming $\alpha = 0.5$ and $\varepsilon = 0.32$. Figure 11 presents the response obtained from vanishing initial conditions, except for $x_0^{(11)} = 0.5$. Besides the map showing how the system response evolutes, the figure presents the spatiotemporal pattern represented by the overlap of 30 iterations during transient and steady state conditions. The results show that the system presents a chaotic response but, after around 5000 iterations, it stabilizes in a periodic response. This kind of behavior may be understood as transient chaos, because the greatest Lyapunov exponent remains stable and positive during this period and, afterwards, becomes zero.

Let us now consider a finite boundary condition with $\alpha = 0.8$ and $\varepsilon = 0.25$. In order to analyze this situation, three different, but close, initial conditions are treated: $x_0^{(11)} = 0.3$, $x_0^{(11)} = 0.4$ and $x_0^{(11)} = 0.5$, vanishing all other cells for all cases, presented in figures 12(a)–(c), respectively. A period-8 response occurs for the first case ($x_0^{(11)} = 0.3$) with $h = 0$. By assuming $x_0^{(11)} = 0.4$, the second case, the system presents a period-4 response with $h = 0$. Nevertheless, by considering $x_0^{(11)} = 0.5$, a chaotic response appears presenting

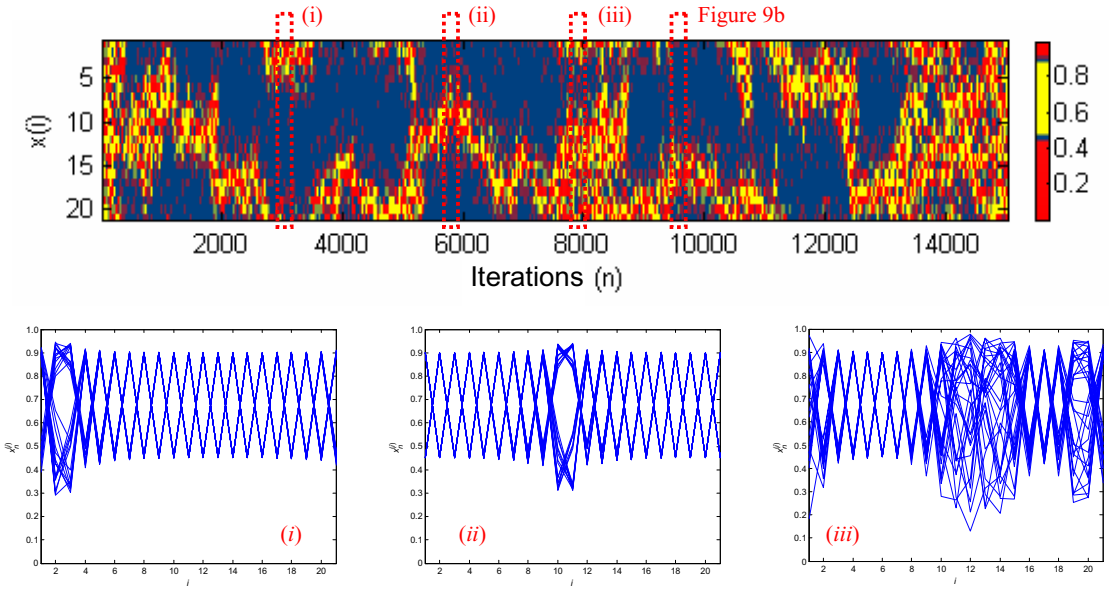

Figure 10. Map showing the movement of the chaotic wave within a period-2 response.

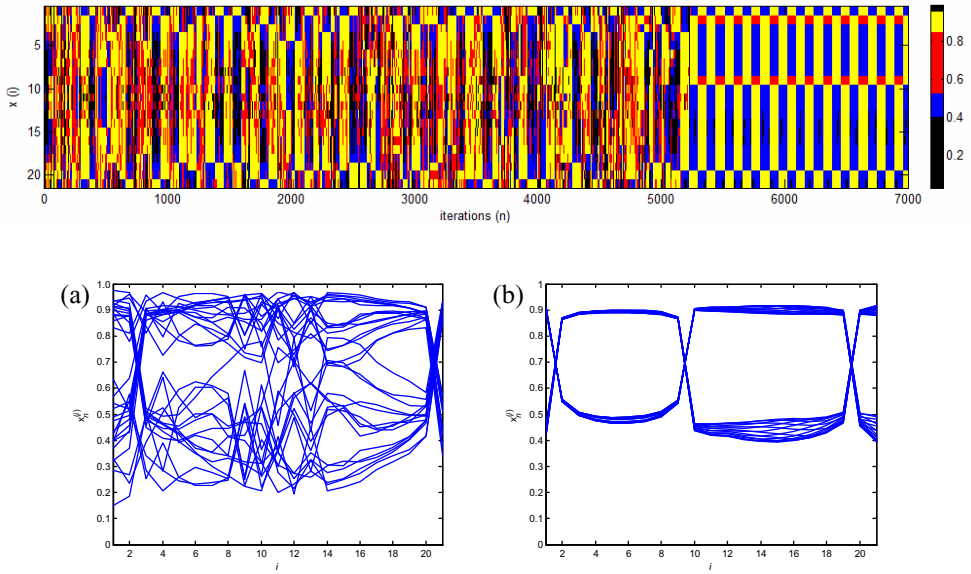

Figure 11. Map showing (a) transient chaos and (b) periodic steady state response for $x_0^{(17)} = 0.5$ (vanishing all other cells).

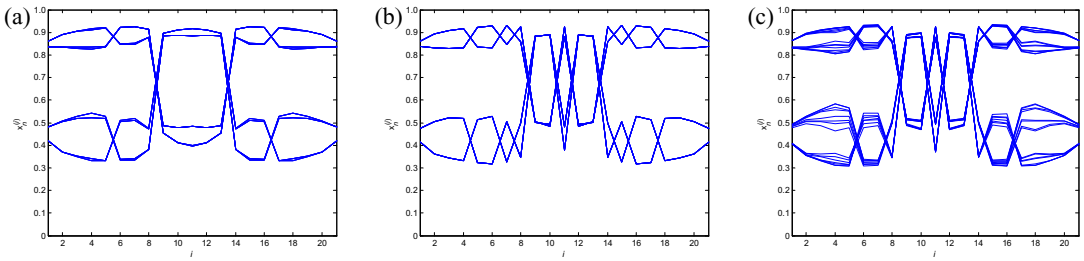

Figure 12. Overlap of the last 30 iterations after 10 000 iterations for finite space boundary response for $\alpha = 0.8$ and $\varepsilon = 0.25$: (a) period-8, (b) period-4 and (c) supertransient chaos.

$h = 0.048$. More than two million iterations are computed in order to observe this response. This phenomenon is probably a case of *supertransient* chaos (Kaneko 1990, 1993, Willeboordse 1992) related to initial conditions that are close to a stable manifold and, as a consequence, the dynamics of the maps takes a long time to leave the chaotic saddle.

5. Non-homogeneous maps

The idea that order and chaos are both related to the complex behavior of physical systems, and that the balance between them occurs in the edge of chaos, motivates the analysis of non-homogeneous systems where transitions between

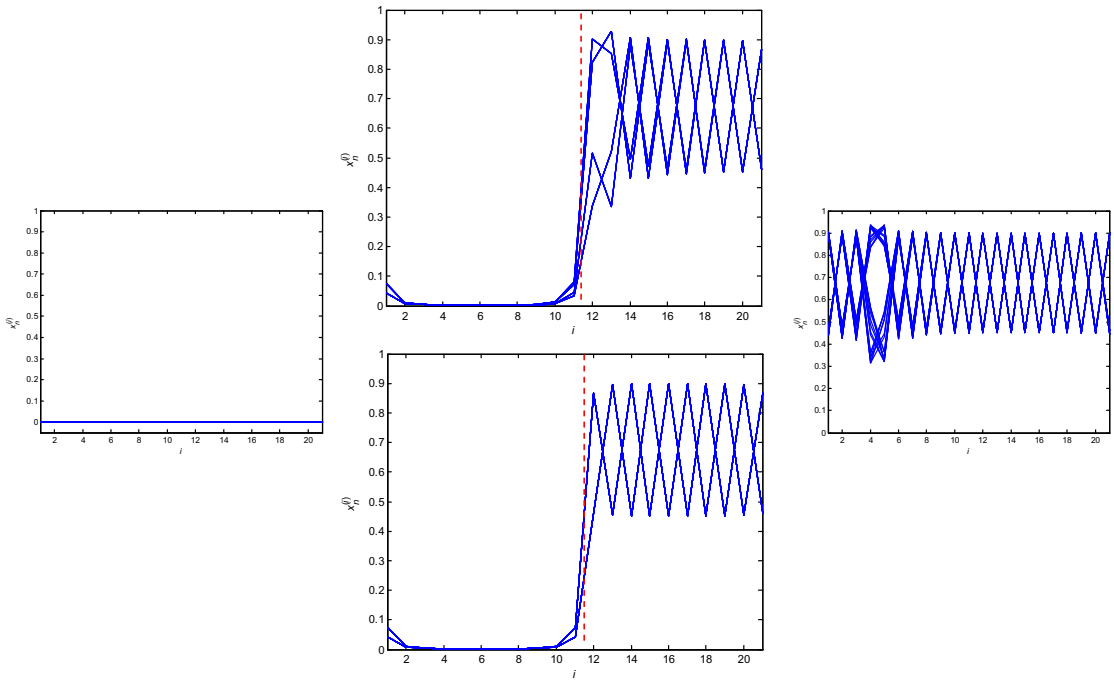

Figure 13. Overlap of the last 30 iterations after 10 000 iterations for $\beta_L = 0$ and $\beta_R = 4$ with periodic boundary conditions, $\alpha = 3$ and $\varepsilon = 0.165$ for two different random initial conditions. The behavior of the homogeneous maps with $\beta = \beta_L$ and $\beta = \beta_R$ is shown on the smaller plots.

different qualitative behavior can result in the emergence of interesting behavior. In this regard, numerical simulations are now carried out by assuming a grid with $N = 21$ and non-homogeneous values of parameter β through the grid. In general, the grid is split into two parts and each one has different values of this parameter. Basically, the idea is to analyze the spatial interaction between two qualitatively different types of behavior. The left side is defined from $i = 1$ to 11, being related to parameter β_L, while the right side is defined from $i = 12$ to 21, being related to parameter β_R. Values of parameter β are chosen in order to consider different qualitative behavior of the isolated map: 0 (period-1, stationary); 3.2 (period-2); 3.5 (period-8); 3.835 (period-3, periodic window); 4 (chaotic). It should be highlighted that three different kinds of responses are possible for the same set of parameters, depending on coupling characteristics: isolated behavior of a single map, homogeneous grid behavior and non-homogeneous grid behavior.

All simulations are conducted assuming that parameter ε is between 0 and 1, while parameter α is between 0 and 3. Three different boundary conditions are focused on: periodic, infinite space and finite space. Moreover, different kinds of initial conditions are imposed on the system.

5.1. Periodic boundary conditions

Initially, let us consider an interaction between two dramatically different types of behavior: stationary ($\beta_L = 0$) and chaotic ($\beta_R = 4$). By assuming coupling parameters $\alpha = 3$ and $\varepsilon = 0.165$, the homogeneous grid with $\beta = 4$ presents chaotic behavior with $h = 0.277$ over a period-2 dynamics. On the other hand, the homogeneous grid dynamics with $\beta = 0$ is stationary. By considering the non-homogeneous case, this pattern is altered due to the interaction of both sides. Figure 13 presents the response of this non-homogeneous grid for two different random initial conditions. Basically, the system response shows period-4 behavior together with a dominant period-2 response. It should be highlighted that this figure also presents the response for the homogeneous grid (small pictures at the left and right sides).

A global analysis of the grid with $\beta_L = 0$ and $\beta_R = 4$ is carried out through the observation of entropy density surface (figure 14). Firstly, let us explain the value where the entropy density tends to $\varepsilon = 0$: it is the average value of the Lyapunov exponents of isolated maps, i.e. 0.69 for the last ten maps and zero for the first 11 maps, that gives $\sim$0.33. The most important observation can be made in the region with strong couplings represented by high values of coupling parameters. Under this condition, the entropy density of the non-homogeneous grid is positive for parameter combinations where the homogeneous grid with $\beta = 4$ has entropy equal to zero. Therefore, the inclusion of the grid with $\beta = 0$ is not related to chaos suppression. Figure 14 also shows details of situations where the non-homogeneous grid presents higher entropy when compared to the homogenous grid, illustrating the preceding comment. A periodic valley is also noticeable around $\varepsilon = 0.05$ and at low values of α, where the grid dynamic develops period-3 and period-6 behavior.

A situation where $\beta_L = 3.2$ (related to period-2 behavior for the isolated map) and $\beta_R = 4$ (chaos) is now the focus. By assuming coupling characteristics represented by $\alpha = 3$ and $\varepsilon = 0.165$, homogeneous behavior is related to period-2 and chaotic behavior (as depicted in figure 15). The interaction of these grids generates a non-homogeneous response that develops chaotic behavior ($h = 0.0134$), although it is highly

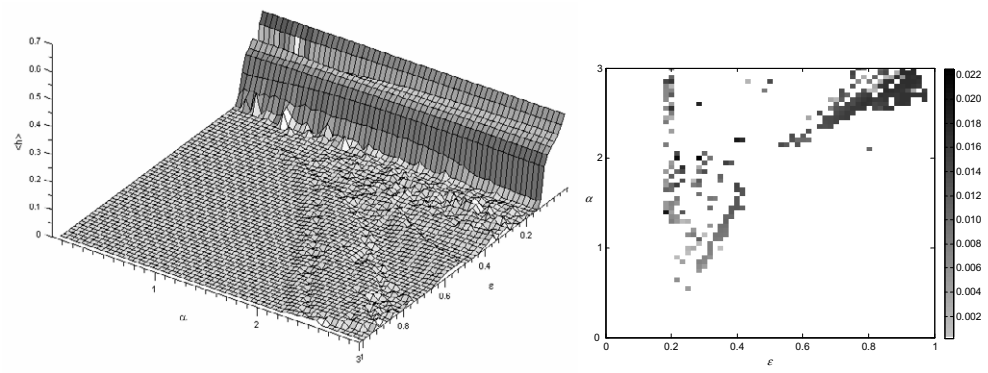

Figure 14. Entropy density surface for $\beta_L = 0$ and $\beta_R = 4$. On the right, regions where the entropy of the non-homogeneous grid is higher than that of the homogeneous grid are highlighted.

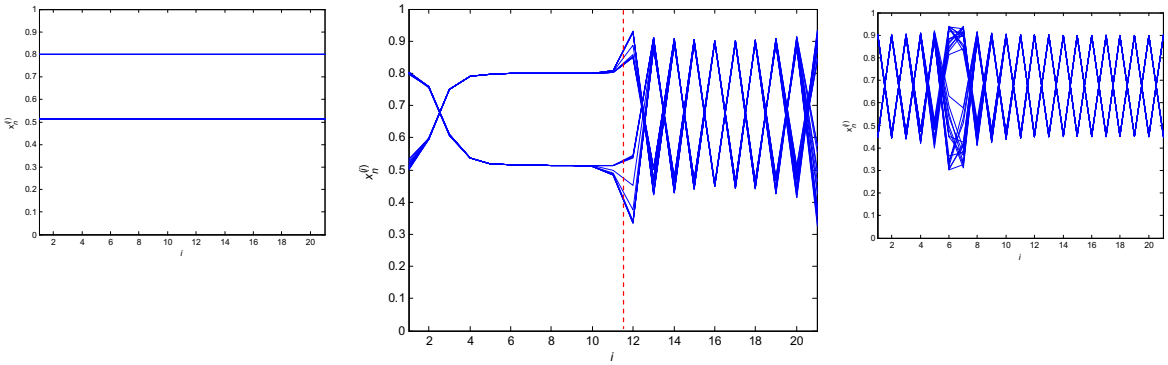

Figure 15. Overlap of the last 30 iterations after 10 000 iterations for $\beta_L = 3.2$ and $\beta_R = 4$, periodic boundary condition, $\alpha = 3$ and $\varepsilon = 0.165$. Random initial conditions. The behavior of homogeneous maps with $\beta = \beta_L$ and $\beta = \beta_R$ is shown on the smaller plots.

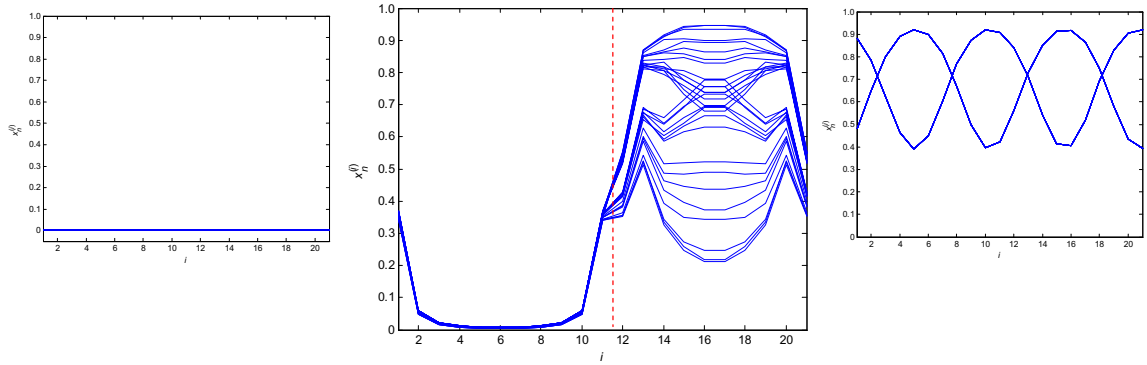

Figure 16. Overlap of the last 30 iterations after 10 000 iterations for $\beta_L = 0$ and $\beta_R = 3.835$, periodic boundary condition, $\alpha = 3$ and $\varepsilon = 0.8$. Random initial conditions. The behavior of homogeneous maps with $\beta = \beta_L$ and $\beta = \beta_R$ is shown on the smaller plots.

suppressed by period-2 on the left side of the grid. This observation shows that when the β_L parameter is changed from zero to 3.2, although this value is related to periodic behavior, the non-homogeneous grid becomes chaotic (figure 15).

By considering $\beta_L = 0$ (stationary) and $\beta_R = 3.835$ (period-3 window) and strong coupling, represented by $\alpha = 3$ and $\varepsilon = 0.8$, homogeneous grids are related to stationary behavior on the left side and period-2 behavior on the right side (as depicted in figure 16). The non-homogeneous grid has a chaotic pattern, as shown in figure 16. The transition between grid sides shows a smoother change of pattern, typical of strong coupling. This observation shows a situation where the chaotic pattern emerges from maps with periodic behavior.

In general, it is possible to say that the periodic boundary condition tends to equalize the dynamics through the grid, mainly with respect to the presence of chaos, due to interaction between two sides of the grid. Chaos in one half and pure periodic motion in the other half is not achievable due to global coupling, even if applied with low intensity and coverage. This behavior points to a transition region where different patterns that can be identified as the edge of chaos could emerge.

5.2. Infinite space boundary condition

Our focus is now on the infinite space boundary condition. This kind of condition imposes synchronized behavior at the boundaries that follows the boundary of each sector. Our

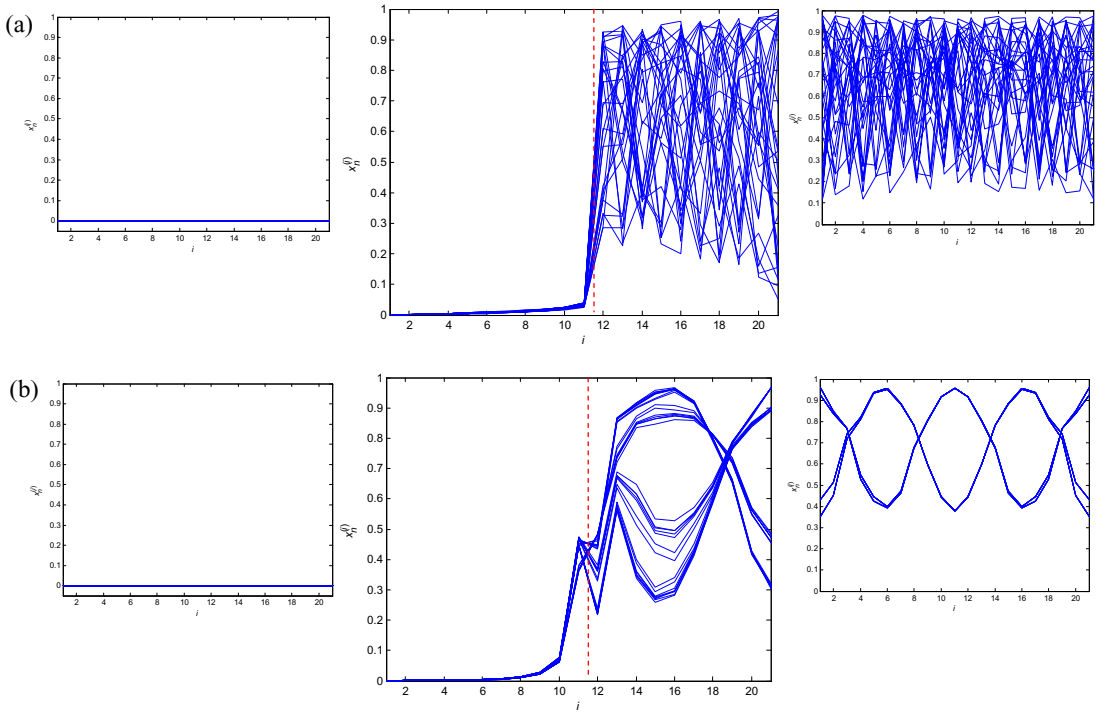

Figure 17. Overlap of the last 30 iterations after 10 000 iterations for $\beta_L = 0$ and $\beta_R = 4$, infinite space boundary condition: (a) $\alpha = 1$, $\varepsilon = 0.1$ and (b) $\alpha = 3$, $\varepsilon = 1$. Random initial conditions. The behavior of homogeneous maps with $\beta = \beta_L$ and $\beta = \beta_R$ is shown on the smaller plots.

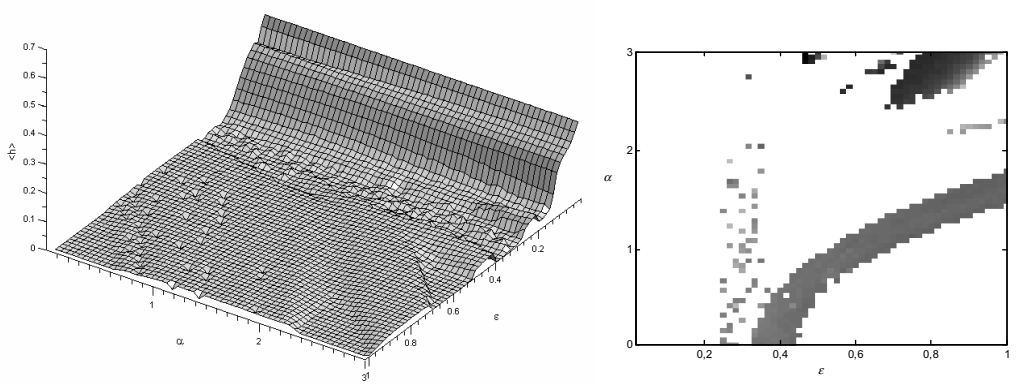

Figure 18. Entropy density surface for $\beta_L = 0$ and $\beta_R = 4$. On the right, regions where the entropy of the non-homogeneous grid is higher than that of the homogeneous grid are highlighted.

analysis starts with the case where $\beta_L = 0$ and $\beta_R = 4$. Two different sets of coupling parameters are chosen: $\alpha = 1$, $\varepsilon = 0.1$ (weak coupling) and $\alpha = 3$, $\varepsilon = 1$ (strong coupling). The first set is a weak coupling and tends to preserve the isolated characteristic of each side (figure 17(a)). The chaotic pattern developed on the right side of the grid is weakly spread to the left side. The interface between both sides shows a sudden increase of amplitude, but the global dynamics is chaotic with $h = 0.1787$. The second set of coupling parameters can be considered as strong coupling and the system tends to a chaotic pattern that can be considered as well organized when compared with the previous one, as shown in figure 17(b), and represented by $h = 0.0056$.

The observation of the entropy surface allows a global analysis of the grid divided into $\beta_L = 0$ and $\beta_R = 4$ (figure 18). If it is compared with the homogeneous grid surface with $\beta = 4$, the first difference between them is that the zero entropy valley does not exist anymore. Chaos suppression in this region no longer occurs when the grid is non-homogeneous. For $\varepsilon = 0$, the entropy is the same as those with periodic boundary conditions, since the absence of coupling makes the boundary condition useless.

At this point, let us observe the grid with $\beta_L = 0$ and $\beta_R = 3.835$ (inside the period-3 window of a single isolated map). Initially, weak coupling ($\alpha = 0.1$ and $\varepsilon = 0.005$) is considered in order to induce period-3 behavior on the left side of the grid and evaluate how the spatial transition would occur (figure 19). It can be observed that both ends tend to behave as homogeneous maps due to the weak coupling. On the right end, a period-3 pattern can be clearly observed (with low chaotic modulation). Despite both sides tending to develop periodic response, there is a chaotic pattern associated

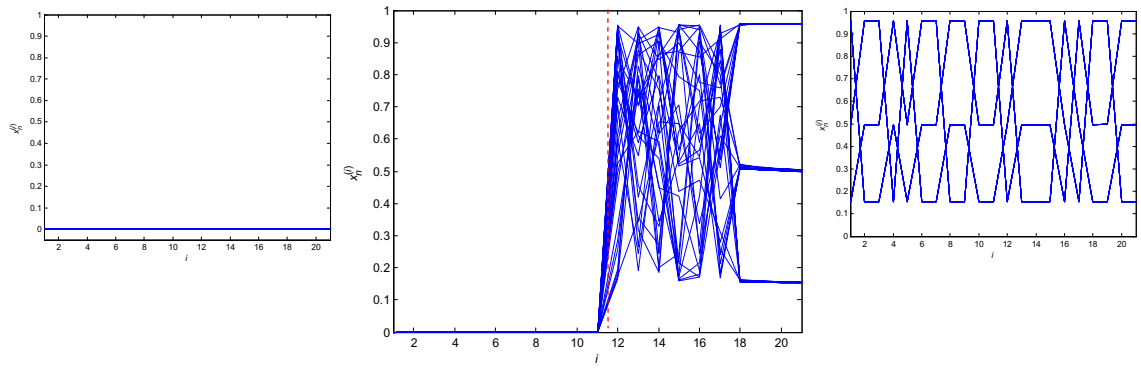

Figure 19. Overlap of the last 30 iterations after 10 000 iterations for $\beta_L = 0$ and $\beta_R = 3.835$, infinite space boundary condition, $\alpha = 0.1$ and $\varepsilon = 0.005$. Random initial conditions. The behavior of homogeneous maps with $\beta = \beta_L$ and $\beta = \beta_R$ is shown on the smaller plots.

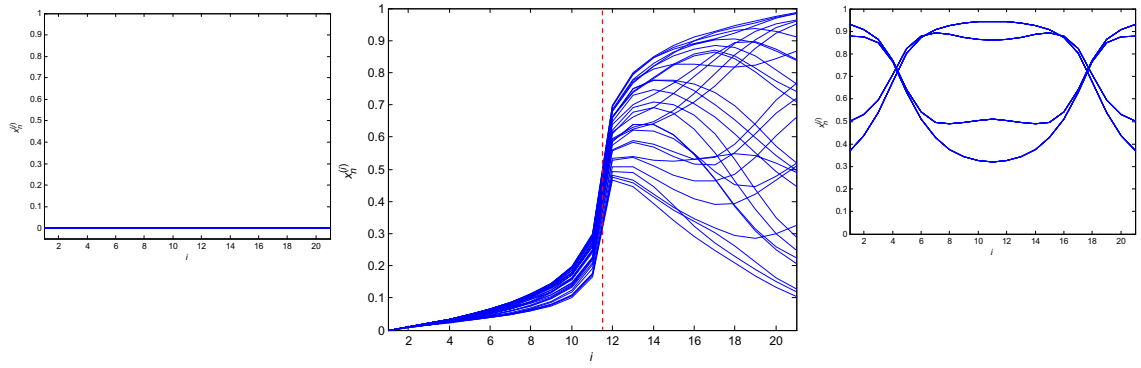

Figure 20. Overlap of the last 30 iterations after 10 000 iterations for $\beta_L = 0$ and $\beta_R = 4$, infinite space boundary condition, $\alpha = 1$ and $\varepsilon = 0.6$. Random initial conditions. The behavior of homogeneous maps with $\beta = \beta_L$ and $\beta = \beta_R$ is shown on the smaller plots.

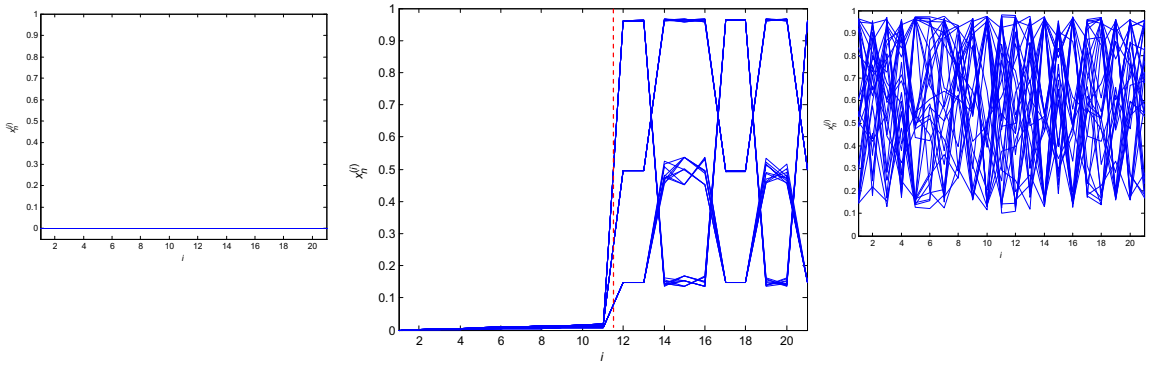

Figure 21. Overlap of the last 30 iterations after 10 000 iterations for $\beta_L = 0$ and $\beta_R = 4$, finite space boundary condition, $\alpha = 0.1$ and $\varepsilon = 0.056$. Random initial conditions. The behavior of homogeneous maps with $\beta = \beta_L$ and $\beta = \beta_R$ is shown on the smaller plots.

with the non-homogeneous behavior ($h = 0.141$). Once again, spatial transitions induce a different kind of pattern.

A similar situation occurs when a grid with $\beta_L = 0$, $\beta_R = 4$, and with coupling represented by $\alpha = 1$ and $\varepsilon = 0.6$, is considered. Under this condition, homogeneous grids with $\beta = 0$ and 4 present periodic responses as depicted in figure 20. For a non-homogeneous grid, the interaction between periodic responses makes a chaotic pattern emerge with $h = 0.0157$, as shown in figure 20.

5.3. Finite space boundary condition

The finite space boundary condition tends to be more restrictive with respect to chaos development. Initially, our analysis considers a critical situation with $\beta_L = 0$ and $\beta_R = 4$. If the coupling is weak, the dynamics becomes closer to the period-3 dynamics. Specifically with coupling parameters $\alpha = 0.1$ and $\varepsilon = 0.05$, a homogeneous map is stationary at the left side and chaotic at the right side (as depicted in figure 21). Concerning non-homogeneous behavior, a chaotic response is observed ($h = 0.0328$); however, a well-organized pattern is clearly identified as being related to a period-3 dominant response (figure 21).

The analysis of the entropy surface allows one to have a better understanding of the system response of the grid with $\beta_L = 0$ and $\beta_R = 4$ (figure 22). It confirms that this boundary condition tends to promote chaos suppression; however, the entropy surface shows regions with positive entropy, mainly when $\alpha > 2$ or for lower values of ε. Once again, when $\varepsilon = 0$, the entropy tends to 0.33. A valley can be noted around $\varepsilon =$

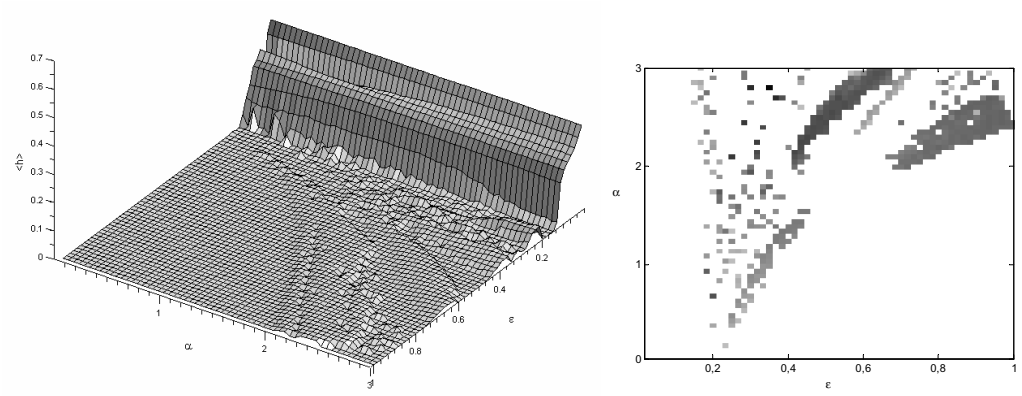

Figure 22. Entropy density surface for $\beta_L = 0$ and $\beta_R = 4$. On the right, regions where the entropy of the non-homogeneous grid is higher than that of the homogeneous grid are highlighted.

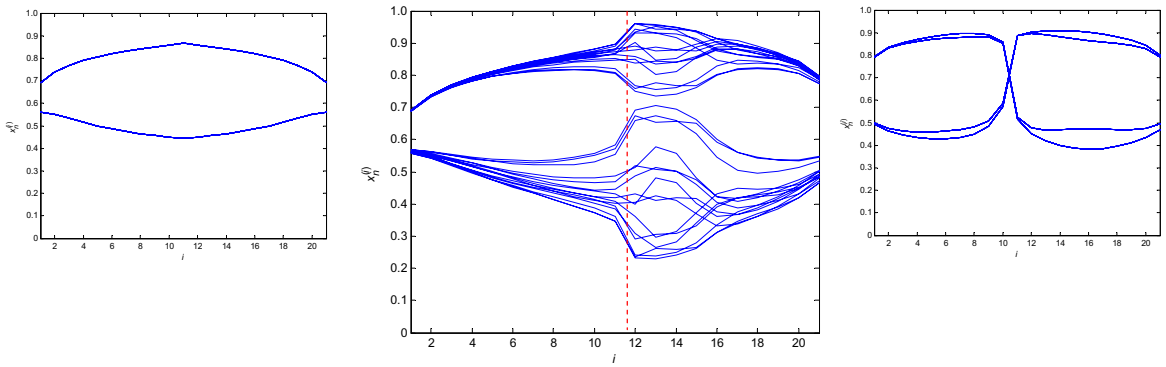

Figure 23. Overlap of the last 30 iterations after 10 000 iterations for $\beta_L = 3.5$ and $\beta_R = 4$, finite space boundary condition, $\alpha = 0.7$ and $\varepsilon = 0.4$. Random initial conditions. The behavior of homogeneous maps with $\beta = \beta_L$ and $\beta = \beta_R$ is shown on the smaller plots.

0.05, where the grid develops period-3 response with chaotic modulation. Figure 22 establishes a comparison between homogeneous and non-homogeneous grids, highlighting regions where the entropy of the non-homogeneous grid is higher than that of the homogeneous grid.

Although periodic boundary conditions tend to suppress chaos, there are situations where two types of periodic behavior induce chaos. In this regard, parameters $\beta_L = 3.5$ and $\beta_R = 4$ are considered with coupling $\alpha = 0.7$ and $\varepsilon = 0.3$. Under this assumption, the homogeneous behavior related to $\beta = 3.5$ presents a period-2 response while $\beta = 4$ is related to period-4 behavior. The non-homogeneous response is chaotic ($h = 0.0101$), as shown in figure 23.

In order to analyze how an isolated map influences a non-homogeneous grid, we assume that maps are gradually inserted into the grid. Under this condition, we assume a homogeneous grid with $\beta = 4$, and isolated maps with $\beta = 3.5$ are inserted substituting the original maps. The entropy density is evaluated after each insertion that is done from map $i = 1$ through $i = 21$ successively. Figure 24 presents this analysis, showing that when nine maps are inserted, the grid starts to develop chaos ($h = 0.0140$). With more than 13 maps, the grid returns to a periodic pattern. This observation shows the spatiotemporal instability of chaos.

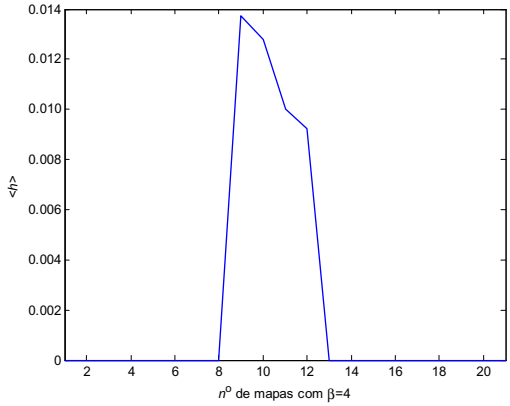

Figure 24. Kolmogorov–Sinai entropy versus number of maps with $\beta = 3.5$ inserted into a homogeneous grid with $\beta = 4$.

6. Conclusions

This paper deals with the spatiotemporal dynamics of coupled logistic maps. The Kolmogorov–Sinai entropy density is used to quantify the complexity of system behavior, permitting a general qualitative understanding of system dynamics. An investigation of different aspects of system dynamics is performed, including different boundary and initial conditions. The influence of boundary conditions increases as the coupling becomes stronger and broader. Periodic boundary conditions present a flat region in the entropy

density surface, and there is a strong tendency for the system to develop synchronized dynamics through all maps. The infinite space boundary conditions show a greater tendency to develop chaos compared to other boundary conditions. This is probably due to the synchronized dynamics imposed by the boundary conditions. The last boundary condition analyzed is finite space and, under this condition, the system shows a weak tendency to become chaotic. The zero value assumed for the outside maps tends to cause a decrease of values along the iterations. Besides the boundary conditions, the influence of initial conditions is treated, presenting an important influence on system dynamics. This influence depends on the boundary conditions. When periodic boundary conditions are assumed, the pattern of the response does not vary with initial conditions, but moves along the maps during the iterations. Transient chaos is observed in systems with infinite space boundary conditions. The finite space boundary conditions are related to the possibility of supertransient chaos. The behavior of non-homogeneous grids shows how distinct types of behavior can interact through spatiotemporal dynamics. In general, the space is split into two parts, and different qualitative responses are considered in each part. Basically, it is possible to observe situations where a chaotic pattern can emerge from two periodic responses and also situations where a periodic pattern can emerge from chaos. This kind of analysis shows how richness is able to emerge in complex systems even in situations where regular dynamics is expected. Of special interest is the transition region that can be identified as the edge of chaos where a rich pattern can emerge assuming distinct responses when compared with the original ones.

Acknowledgments

We acknowledge the support of the Brazilian Research Councils CNPq and FAPERJ.

References

Awrejcewicz J 1991 Nonlinear dynamics of a two-body nonlinear mechanical system *Comput. Methods Appl. Mech. Eng.* **91** 1093–108

Batista A M and Viana R L 2001 Lyapunov exponents of a lattice of chaotic maps with a power-law coupling *Phys. Lett.* A **286** 134–40

Chazottes J-R and Fernandes B 2005 *Dynamics of Coupled Map Lattices and Related Spatially Extended Systems* (*Lecture Notes in Physics* vol 671) (Berlin: Springer)

Giordani F T and da Silva J A L 2005 Sincronização em metapopulações com migração dependente da densidade *TEMA Tend. Mat. Apl. Comput.* **6** 229–37

Holden A V and Zhang H 1992 Lyapunov exponent spectrum for a generalized coupled map lattice *Chaos Solitons Fractals* **2** 155–64

Kaneko K 1990 Supertransients, spatiotemporal intermittency and stability of fully developed spatiotemporal chaos *Phys. Lett.* A **149** 105–12

Kaneko K 1993 *Theory and Applications of Coupled Map Lattices* (New York: Wiley)

Kozma R 1998 Intermediate-range coupling generates low-dimensional attractors deeply in the chaotic region of one-dimensional lattices *Phys. Lett.* A **244** 85–91

Lai Y C and Grebogi C 1999 Modeling of coupled chaotic oscillators *Phys. Rev. Lett.* **82** 4803–6

Li J-H 2008 Globally coupled chaotic maps with constant force *Commun. Theor. Phys.* **49** 665–8

Lloyd A L 1995 The coupled logistic map: a simple model for the effects of spatial heterogeneity on population dynamics *J. Theor. Biol.* **173** 217–30

Lu J, Yang G, Oh H and Luo A C J 2005 Computing Lyapunov exponents of continuous dynamical systems: method of Lyapunov vectors *Chaos Solitons Fractals* **23** 1879–92

May R M 1976 Simple mathematical models with very complicated dynamics *Nature* **261** 459–67

Savi M A 2007 Effects of randomness on chaos and order of coupled logistic maps *Phys. Lett.* A **364** 389–95

Shen Y, Hou Z H and Xin H W 2008 Synchronization and pattern dynamics of coupled chaotic maps on complex networks *Chin. Phys. Lett.* **25** 3875

Shibata H 1998a Quantitative characterization of spatiotemporal patterns *Physica* A **253** 134–142

Shibata H 1998b Quantitative characterization of spatiotemporal chaos *Physica* A **253** 428–49

Shibata H 2001 KS entropy and mean Lyapunov exponent for coupled map lattices *Physica* A **292** 182–92

Umberger D K, Grebogi C, Ott E and Afeyan B 1989 Spatiotemporal dynamics in a dispersively coupled chain of nonlinear oscillators *Phys. Rev.* A **39** 4835–42

Vasconcelos D B, Viana R L, Lopes S R, Batista A M and Pinto S E de S 2004 Spatial correlations and synchronization in coupled map lattices with long-range interactions *Physica* A **343** 201–18

Viana R L, Grebogi C, Pinto S E de S, Lopes S R, Batista A M and Kurths J 2005 Bubbling bifurcation: loss of synchronization and shadowing breakdown in complex systems *Physica* D **206** 94–108

Willeboordse F 1992 Selection of windows, attractors and self-similar patterns in a coupled map lattice *Chaos Solitons Fractals* **2** 609–34

Willeboordse F H 2003 The spatial logistic map as a simple prototype for spatiotemporal chaos *Chaos* **13** 533–40

Wolf A, Swift J B, Swinney H L and Vastano J A 1985 Determining Lyapunov exponents from a time series *Physica* D **16** 285–317

Wysham D B and Hastings A 2008 Sudden shifts in ecological systems: intermittency and transients in the coupled ricker population model *Bull. Math. Biol.* **70** 1013–31